



Shahid Chamran
University of Ahvaz

Journal of Applied and Computational Mechanics



Research Paper

Numerical Investigation on Flow Transition through a Curved Square Duct with Negative Rotation

Mohammad Sanjeed Hasan¹, Shamsun Naher Dolon², Himadri Shekhar Chakraborty³,
Rabindra Nath Mondal⁴, Giulio Lorenzini⁵

¹ Department of Mathematics, Bangabandhu Sheikh Mujibur Rahman Science and Technology University, Gopalganj-8100, Bangladesh, Email: sanjeedhasan@gmail.com

² Department of Mathematics, Jagannath University, Dhaka-1100, Bangladesh, Email: dolonjnu02@gmail.com

³ Department of Mathematics, Shahjalal University of Science and Technology, Sylhet-3114, Bangladesh, Email: himadri-mat@sust.edu

⁴ Department of Mathematics, Jagannath University, Dhaka-1100, Bangladesh, Email: rmondal71@yahoo.com

⁵ Department of Engineering and Architecture, University of Parma, Parma 43124, Italy, Email: giulio.lorenzini@unipr.it

Received May 14 2020; Revised August 04 2020; Accepted for publication August 08 2020.

Corresponding author: M.S. Hasan (sanjeedhasan@gmail.com)

© 2021 Published by Shahid Chamran University of Ahvaz

Abstract. Application of the rotational phenomena in the curved ducts plays an important role in many engineering areas, so researchers are attracted to innovate something new in this area nowadays. In this regard, the current paper has performed the fluid flow through the curved duct for an extensive range of negative rotation ($-10 \leq Tr \leq -1500$). The other useful parameters such as Dean number (Dn), Curvature (δ), Grashof number (Gr), and Prandtl number (Pr) are considered fixed. The investigations are divided into four parts. In the first portion, linear stability of the flows through the duct is discussed. Then time evolution calculations of the unsteady solutions for different Taylor numbers are demonstrated in the “time vs. heat flux” plane. This inquiry shows that the flow undergoes various instabilities for increasing the Taylor number. Thirdly, two types of flow velocity, axial flow and secondary flow and the temperature profiles are represented. It is obtained that two up to six vortex secondary flows are found for the regular and irregular oscillation and the flow patterns are different for a fixed period for regular oscillation. To show more clarity of the periodic and chaotic flow, power spectrum density is further examined. However, it is observed that the flows are mixed and enhanced heat transfer because of the acting of centrifugal force, Coriolis force, and heating induced buoyancy force on the duct. Finally, the numerical results are compared with the experimental data which shows that the numerical data fully matches with the experimental outcome.

Keywords: Linear stability, Secondary flow, Time-dependent solutions, Power spectrum density, Experimental results.

1. Introduction

Curved duct flows are incredibly used in the engineering applications such as gas turbines blades, heat exchangers, lab-on-a-chip device, aircraft engineering, nuclear reactors, solar energy system, plastic industry, cooling on smart vessels. The duct which is rolling with a specific axis is known as a rotational duct and when the duct is rotated reversely to z-axis then it is acquainted as a negative rotational duct. There are various shapes in a curved square duct, for example, S-shaped duct, U-shaped duct, Y-shaped duct, cylindrical duct, semi-circular duct, V-shaped duct, elliptical duct, square and rectangular duct, twisted duct, etc. Among them, some excellent cited article on curved ducts are given by Elsamni et al. [1], Du et al. [2], Chandratilleke and Nadim [3], Mondal et al. [4], Anand and Sandeep [5], Fiola and Agarwal [6], Rumsey et al. [7], Chamkha et al. [8]. To investigate various phenomena in a curved duct, scholars are very much attracted to examine the solution structure as well as the linear stability. Very recently, Nowruzi et al. [9] have reported to find out the effect of hydrodynamic instability through duct for a wide range of aspect ratio (from 0.2 to 2) by using energy gradient method. Linear stability theory for two and three-dimensional cases have been demonstrated by Watanabe et al. [10]. They further obtained a relation between linear stability and the time-dependent solution. A detailed study of linear stability for isothermal flows through curved square duct has been carried out by Mondal et al. [11]. Here, all authors have conducted their work for rotational and non-rotational case. But stability analysis for negative rotation has not been done yet. The ongoing paper has first illustrated the linear stability analysis for negative rotation.

To change the flow structure with respect to the time is another important objective in mechanics because it is widely used in metallic industry and other fields of biomedical engineering. Time-dependent behaviors with respect to the drag and the lift coefficient have been narrated by Nazeer et al. [12]. Using flow visualization and computational fluid dynamics techniques, Krishna et al. [13] studied the unsteady solution for fixed curvature 0.3. For both positive and negative rotation, various types of flow patterns were obtained by Islam et al. [14]. Time-dependent oscillations for rotating duct have been detected for different curvatures and a wide range of Taylor number by Sultana et al. [15]. They have also shown an unsteady diagram in the Tr vs.



Curvature plane for both positive and negative rotation. Hasan et al. [16] represented a relation between the bifurcation structure and the unsteady flow behavior through non-rotating curved duct. They observed that the irregular oscillation has come after the steady-state and regular oscillation respectively. Dynamic responses of the flow through a curved duct have been visualized by Wang et al. [17]. Chamkha et al. [18] considered a magnetic field in a rotating vertical cone and observed the time-dependent fluctuation of angular velocity with respect to different temperatures. An outstanding concept on the flow transition for curved rectangular duct has been described by Yanase et al. [19]. They tried to get a strong connection between the steady branches and the time evolution calculation. Later, Mondal et al. [20-21] considered the Adam Bashforth method together with function collocation method to examine the unsteady behavior only for the positive rotation. In their research, they revealed the phase space to be sure about the periodic, multi-periodic and chaotic flows. But in the entire cited paper, they did not disclose the power spectrum density where power spectrum density is an important tool for finding out whether the flow oscillates or non-oscillate. The present study has filled up this gap.

It is alluded that the governing equation of the flows through the curved duct was first introduced by Dean [22]. He also discussed that there are two types of forces are acted in the curved square duct. One is the centrifugal force and the other is body force. By simplifying his equation subsequently, another parameter was produced, which has addressed as the Coriolis force. Here, the centrifugal force is produced from the curvature of the duct and the Coriolis force is affected by the rotation of the duct. For small Reynold number, Harding et al. [23] focused on the acting forces in a spherical particle suspended in the flow-through square, rectangular and trapezoidal cross-section of the duct. Using pressure gradient method, Nowruzi et al. [24] obtained various types of flow patterns. They have also validated their results with the experimental data. The vector plot of the secondary flow where suction blow process has been also produced has been drawn by Kabanemi et al. [25] numerically. By applying flow visualization and computational fluid dynamics technique to perform the flow structures in a curved pipe have been conducted by Krishna et al. [13] where the feature of the secondary flow and the regions of the boundary layer separation have been illustrated by Fiola and Agarwal [6]. Parvin et al. [26] revealed the different types of parameter effects in secondary flow including Grashof number and Prandtl number where they considered the nanoparticles through the annulus. Recently, Mondal et al. [27] got two to ten vortex secondary flows for large aspect ratio 4. They have also shown in the *Grashof number vs. aspect ratio* plane that for increasing the required parameters, the number of vortexes has enhanced. Dolon et al. [28] exposed the flows with changing the Dean number for the non-isothermal case. They have also delivered a clear idea about Dean vortex. Arifuzzaman et al. [29] tried to give a detailed explanation of centrifugal and Coriolis effect in the unsteady flows on the curved square duct. Two- and three-dimensional flow patterns through the duct have been first manifested by Yanase et al. [30]. Numerical as well as an experimental investigation of the flow have been first carried out by Yamamoto et al. [31]. Nivedita et al. [32] analyzed the influence of vortices in cell separation through the spiral duct for different Reynolds numbers. The experimental results for both positive and negative rotation have first exhibited by them. Here, most of the cited paper has not explored the axial flow, but the present study has shown the secondary flow, temperature profile along with this kind of flow velocity. Besides, the secondary flows have been validated with the experimental result.

Analyzing heat transfer in curved ducts is an important issue because it helps to elucidate the stability and the flow variation easily. Yanase et al. [33] assayed to give a clear idea of heat transfer and the temperature gradients for rectangular duct. They have expressed the figure with the help of the steady branches as well as the average of unsteady solution. Later, Mondal et al. [34] accomplished almost the same work for square duct. Very recently, Du et al. [2] calculated flow and heat transfer for fixed Reynold number (7000) where the rotational number is varied from 0 to 1. Umavathi et al. [35] studied the influence of viscosity in the horizontal channel temperature and the flow velocity. Chandratilleke et al. [36] displayed the heat transmission among the elliptical and rectangular duct for both numerically and experimentally. Hasan et al. [37-38] narrated the heat transfer as well as the temperature gradient for both rotating and non-rotating curved square duct.

In the existent study, the governing equation of the curved duct has been formulated first and then the numerical accuracy has been presented. Then, in the result and discussion section, linear stability, time-history analysis with the velocity and temperature profiles of the curved square duct has been performed for an extensive range of negative rotation. Furthermore, validation of numerical results with the experimental data has been also represented. The outcomes of the investigation and the applications have been included in brief at concluding remarks.

2. Governing Equations

Figure 1 illustrates a two-dimensional rotating curved duct model that can rotate in both positive and negative direction along the z' – axis. The fluid flow goes through the duct and the fluid is considered as viscous incompressible. As the article is based on the square duct so the height and width of the duct are equal. The temperature is conducted at the lower wall of the duct and the other walls are at room temperature. So it can be said that the body heat at the lower wall of the duct is $T_0 + \Delta T$, where $\Delta T > 0$. Here, x' and y' are assumed in the horizontal and vertical directions consecutively. For two-dimensional flow, the axial flow moves with a fixed pressure gradient, G , along the centerline which is taken to be in z' – direction. The required non-dimensional governing equations are represented as:

Continuity equation:

$$\frac{\partial u'}{\partial r'} + \frac{\partial v'}{\partial y'} + \frac{u'}{r'} = 0, \quad (1)$$

Momentum equations:

$$\frac{\partial u'}{\partial t'} + u' \frac{\partial u'}{\partial r'} + v' \frac{\partial u'}{\partial y'} - \frac{w'^2}{r'} = -\frac{1}{\rho} \frac{\partial P'}{\partial r'} + v \left[\frac{\partial^2 u'}{\partial r'^2} + \frac{\partial^2 u'}{\partial y'^2} + \frac{1}{r'} \frac{\partial u'}{\partial r'} - \frac{u'}{r'^2} \right], \quad (2)$$

$$\frac{\partial v'}{\partial t'} + u' \frac{\partial v'}{\partial r'} + v' \frac{\partial v'}{\partial y'} = -\frac{1}{\rho} \frac{\partial P'}{\partial y'} + v \left[\frac{\partial^2 v'}{\partial r'^2} + \frac{1}{r'} \frac{\partial v'}{\partial r'} + \frac{\partial^2 v'}{\partial y'^2} \right] + g\beta T', \quad (3)$$

$$\frac{\partial w'}{\partial t'} + u' \frac{\partial w'}{\partial r'} + v' \frac{\partial w'}{\partial y'} + \frac{u'w'}{r'} = -\frac{1}{\rho} \frac{1}{r'} \frac{\partial P'}{\partial z'} + v \left[\frac{\partial^2 w'}{\partial r'^2} + \frac{\partial^2 w'}{\partial y'^2} + \frac{1}{r'} \frac{\partial w'}{\partial r'} - \frac{w'}{r'^2} \right], \quad (4)$$



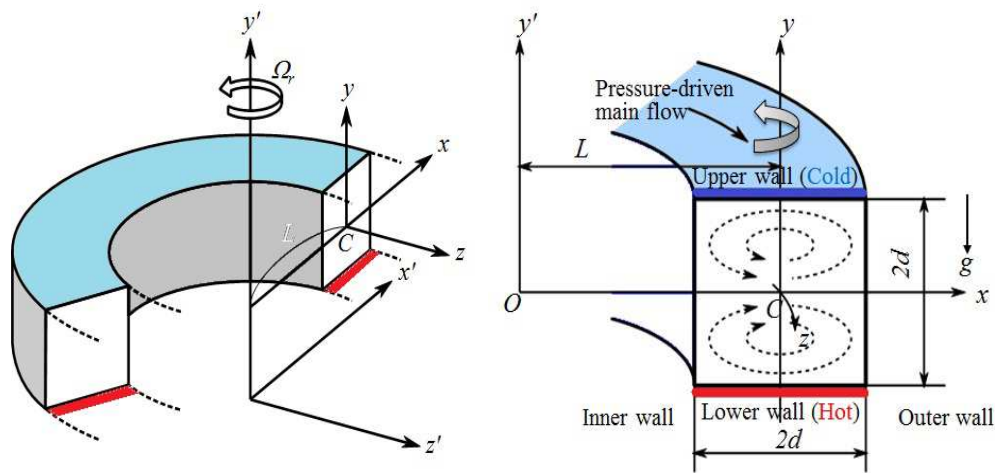


Fig. 1. Co-ordinate system of the rotating curved square duct.

Energy equation:

$$\frac{\partial T'}{\partial t'} + u' \frac{\partial T'}{\partial r'} + v' \frac{\partial T'}{\partial y'} = \kappa \left[\frac{\partial^2 T'}{\partial r'^2} + \frac{1}{r'} \frac{\partial T'}{\partial r'} + \frac{\partial^2 T'}{\partial y'^2} \right], \quad (5)$$

Here, the velocity components u' , v' , w' are worked in x' , y' , z' -axis respectively. The notations P' , T' , and t' are addressed respectively as dimensional pressure, temperature and time and the Greek notations ρ , ν , β , κ and g are named as density, kinematic viscosity, coefficient of thermal expansion, coefficient of thermal diffusivity and gravitational acceleration consecutively. The dimensional variables have been nondimensionalized by using the representative length d , the representative velocity $U_0 = \nu / d$, where ν is the kinematic viscosity of the fluid. The non-dimensional variables are as follows:

$$u = \frac{u'}{U_0}, \quad v = \frac{v'}{U_0}, \quad w = \frac{\sqrt{2\delta}}{U_0} w', \quad x = \frac{x'}{d}, \quad \bar{y} = \frac{y'}{d}, \quad z = \frac{z'}{d}, \quad T = \frac{T'}{\Delta T'}, \quad t = \frac{U_0}{d} t', \quad \delta = \frac{d}{L}, \quad P = \frac{P'}{\rho U_0^2}, \quad G = -\frac{d}{\rho U_0^2} \frac{\partial P'}{\partial y'}$$

The representative velocity U_0 is identified as $U_0 = \nu / d$ and the stream function (ψ) is defined as

$$u = \frac{1}{1 + \delta x} \frac{\partial \psi}{\partial y} \quad \text{and} \quad v = -\frac{1}{1 + \delta x} \frac{\partial \psi}{\partial x} \quad (6)$$

Herein, the notation δ is curvature and defined as $\delta = d / L$. After using the non-dimensional variables and stream function in equations (1) to (5) and then simplifying and combining the equations, we get,

$$(1 + \delta x) \frac{\partial w}{\partial t} + \frac{\partial(w, \psi)}{\partial(x, y)} - Dn + \frac{\delta^2 w}{1 + \delta x} = (1 + \delta x) \Delta_2 w - \frac{\delta}{1 + \delta x} \frac{\partial \psi}{\partial y} w + \delta \frac{\partial w}{\partial x} - \delta Tr \frac{\partial \psi}{\partial y} \quad (7)$$

$$\left(\Delta_2 - \frac{\delta}{1 + \delta x} \frac{\partial}{\partial x} \right) \frac{\partial \psi}{\partial t} = -\frac{1}{(1 + \delta x)} \frac{\partial(\Delta_2 \psi, \psi)}{\partial(x, y)} + \frac{\delta}{(1 + \delta x)^2} \left[\frac{\partial \psi}{\partial y} \left(2\Delta_2 \psi - \frac{3\delta}{1 + \delta x} \frac{\partial \psi}{\partial x} + \frac{\partial^2 \psi}{\partial x^2} \right) - \frac{\partial \psi}{\partial x} \frac{\partial^2 \psi}{\partial x \partial y} \right] - \frac{2\delta}{1 + \delta x} \frac{\partial}{\partial x} \Delta_2 \psi + w \frac{\partial w}{\partial y} + \frac{\delta}{(1 + \delta x)^2} \times \left[3\delta \frac{\partial^2 \psi}{\partial x^2} - \frac{3\delta^2}{1 + \delta x} \frac{\partial \psi}{\partial x} \right] + \Delta_2^2 \psi - Gr(1 + \delta x) \frac{\partial T}{\partial x} + \frac{1}{2} Tr \frac{\partial w}{\partial y} \quad (8)$$

$$\frac{\partial T}{\partial t} + \frac{1}{(1 + \delta x)} \frac{\partial(T, \psi)}{\partial(x, y)} = \frac{1}{Pr} \left(\Delta_2 T + \frac{\delta}{1 + \delta x} \frac{\partial T}{\partial x} \right) \quad (9)$$

Here, w , ψ and T are non-dimensional variables. From equation (7) to (9), some new parameters are consisted and parameters are defined as,

$$Dn = \frac{Gd^3}{\mu\nu} \sqrt{\frac{2d}{L}}, \quad Tr = \frac{2\sqrt{2}\delta\Omega_T d^3}{\nu\delta}, \quad Gr = \frac{\beta g \Delta T}{\nu^2} d^3, \quad Pr = \frac{\nu}{\kappa} \quad (10)$$

In equation (10), Dn , Tr , Gr , Pr is the short designation of Dean number, Taylor number, Grashof number and Prandtl number respectively.

Now the boundary conditions for axial (w) and secondary (ψ) flow is

$$w(\pm 1, y) = w(x, \pm 1) = \psi(\pm 1, y) = \psi(x, \pm 1) = \frac{\partial \psi}{\partial x}(\pm 1, y) = \frac{\partial \psi}{\partial y}(x, \pm 1) = 0 \quad (11)$$

and for temperature (T)

$$T(x, 1) = 1, \quad T(x, -1) = -1, \quad T(\pm 1, y) = y \quad (12)$$



There is a group of solutions which satisfy the following symmetry condition with respect to the horizontal plane $y = 0$.

$$\left. \begin{aligned} w(x, y, t) &\Rightarrow w(-x, y, t), \\ \psi(x, y, t) &\Rightarrow -\psi(-x, y, t), \\ T(x, y, t) &= -T(-x, y, t) \end{aligned} \right\} \quad (13)$$

A symmetric solution is found when the solution satisfies the equation (13) and an asymmetric solution appears for all the other cases. In the current study, effects of rotation in negative direction have been represented. So, all parameters are assumed as constant ($Dn = 1000$, $\delta = 0.001$, $Gr = 100$, $Pr = 7.0$ (water)) without the rotational parameter (Taylor number is varied from -10 to -1500).

3. Numerical Calculations

3.1 Method of Numerical Calculations

To calculate the flow behavior numerically, *Spectral method* is considered. This method is mainly based on the expansion of the series. More explicitly, the variables in the governing equations are stretched to series expansion formed with Chebyshev polynomials. The expansion functions $\varphi_n(x)$ and $\psi_n(x)$ are expressed as:

$$\left. \begin{aligned} \varphi_n(x) &= (1 - x^2) C_n(x), \\ \psi_n(x) &= (1 - x^2)^2 C_n(x) \end{aligned} \right\} \quad (14)$$

where, $C_n(x) = \cos(n \cos^{-1}(x))$ is defined as the Chebyshev polynomial of n^{th} order. Here the axial flow (w), stream function (ψ) and isotherms (T) are taken into account as the function of x -axis, y -axis and time respectively and $w(x, y, t)$, $\psi(x, y, t)$, and $T(x, y, t)$ are extended separately in terms of the expansion functions $\varphi_n(x)$ and $\psi_n(x)$ as:

$$\left. \begin{aligned} w(x, y, t) &= \sum_{m=0}^M \sum_{n=0}^N w_{mn}(t) \phi_m(x) \phi_n(y) \\ \psi(x, y, t) &= \sum_{m=0}^M \sum_{n=0}^N \psi_{mn}(t) \psi_m(x) \psi_n(y) \\ T(x, y, t) &= \sum_{m=0}^M \sum_{n=0}^N T_{mn}(t) \varphi_m(x) \varphi_n(y) - y \end{aligned} \right\} \quad (15)$$

Here, M and N represent the grid size in x and y direction consecutively and w_{mn} , ψ_{mn} and T_{mn} are the coefficients of expansion. To seek out the unsteady solution $\bar{w}(x, y)$, $\bar{\psi}(x, y)$ and $\bar{T}(x, y)$, the expansion series (15) is confine into the non-dimensional equations (7) - (9) and the collocation method is then used. As a consequence, a set of nonlinear algebraic equations for w_{mn} , ψ_{mn} and T_{mn} are formed. The collocation points (x_i, y_j) are assumed to be

$$x_i = \cos\left[\pi\left(1 - \frac{i}{M+2}\right)\right], \quad y_j = \cos\left[\pi\left(1 - \frac{j}{N+2}\right)\right] \quad (16)$$

where $i = 1, \dots, M+1$ and $j = 1, \dots, N+1$. For investing the time dependent behavior, the collocation theory is used together with equation (5) and the Crank-Nicolson as well as the Adams-Bashforth methods and then put into equations (7) - (9).

3.2 Grid Efficiency

Here, grid accuracy of the numerical algorithm has been represented. As the paper has illustrated the flow behavior through curved square duct, so the grid sizes are equal. In this investigation, M and N are addressed as the grid size where $M = N$ is considered due to square duct. Table 1 displays the grid accuracy table for different grid sizes with observing the value of heat flux and axial flow. It is certainly said that there is no dramatic change for changing the grid size. To compare more explicitly, percentage relative errors are also calculated, where percent relative error (pre) is designated as, $pre = [(present - previous \text{ value}) / [present \text{ value}]] \times 100\%$. Percentage relative error for both heat flux and axial value demonstrated that for increasing the grid size the errors have been reduced.

Figure 2 exposes the pie chart for the percentage relative error of heat flux and axial flow respectively where the values are taken from the table. It is illustrated from the figure that the accuracy of the algorithm is accurate enough for the large grid sizes. In this study, $M = N = 20$ has been taken, because it gives almost accurate value and reduces the cost.

3.3 Flux Through the channel

In the impending work, the total flux through the channel in the rotating coordinate system is elucidated as,

$$Q' = \int_{-d}^d \int_{-d}^d w' dx' dy' = VdQ \quad (17)$$

Table 1. The values of Q and $w(0, 0)$ for various M and N at $Dn = 1000$, $Gr = 100$, $Tr = -1500$ and $\delta = 0.001$.

M	N	Q	Percentage relative error of Q	$w(0, 0)$	Percentage relative error of w
16	16	261.545967	0.314662	387.844757	0.307387
18	18	262.371550	0.133469	389.040618	0.726774
20	20	262.021832	0.049784	386.233572	0.104173
22	22	262.152341	0.007508	386.636344	0.055168
24	24	262.132659	-----	386.849762	-----



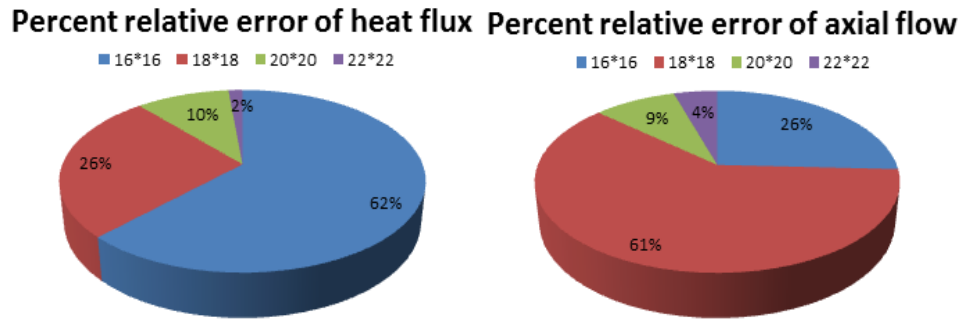


Fig. 2. Pie chart of the grid sizes of percentage relative error.

where, Q' is the dimensional total heat flux and \bar{w}' is the mean axial velocity which is enumerated by,

$$\bar{w}' = \frac{Q'}{4d} \quad (18)$$

However, after dimensionless the equation (17), the total flux Q is written as,

$$Q = \int_{-1}^1 \int_{-1}^1 w dx dy \quad (19)$$

Here, the heat flux is important for investigating the unsteady behavior of the rotating curved duct.

4. Result and Discussion

4.1 Linear stability analysis

Linear Stability of the curved duct of negative rotation is investigated here for an extensive range of Taylor number. In this study, linear stability is enumerated only for two-dimensional cases where the z-axis is assumed as independent. To calculate linear stability, function expansion together with the collocation method is used to the linear perturbation of $\bar{w}(x,y)$ and $\bar{\psi}(x,y)$. The time-dependent of perturbation is considered as $e^{\sigma t}$, where $\sigma = \sigma_r + i\sigma_i$. If all the values of σ_r are negative, then the solution shows linear stability. On the other hand, if σ_r bears single positive value then it reveals linear unstable. In the unstable region, the perturbation generates oscillatory for $\sigma_i \neq 0$ and monotonically for $\sigma_i = 0$. Table 2 displays the linear stability table. Linear stable regions are designated by bold italics sign. It has obtained that linear stable points have occurred between two different regions ($-182.50 \leq Tr \leq -370.99$ & $-590.99 \leq Tr \leq -912.12$). It is also noticed that there is a strong connection between the linear stability and the time-dependent behavior which is shown in the time evolution section. Now, two types of flow velocity axial and secondary flow and their isotherms are shown in Figure 3 for different Taylor number. It is demonstrated that two types of axial flow behavior has been found between $-10 \leq Tr \leq -1500$. From $Tr = -10$ to $Tr \leq -250$, the flow velocity has pushed to the outer wall of the duct while the opposite behavior of axial velocity has been found from $Tr > -250$ to $Tr = -1500$. The secondary flow narrates that two- up to six-vortex flow has built up for the required Taylor number.

4.2 Time Evolution Calculation

In this section, time evolution calculations of the unsteady solution are investigated here for a wide range of negative rotations ($-10 \leq Tr \leq -1500$) where other parameter values are fixed. To find out the data, Code::Blocks works as the subordinate tool, where the algorithm of governing equations is built up with Crank-Nicolson as well as the Adam-Bashforth method together with the function collocation method.

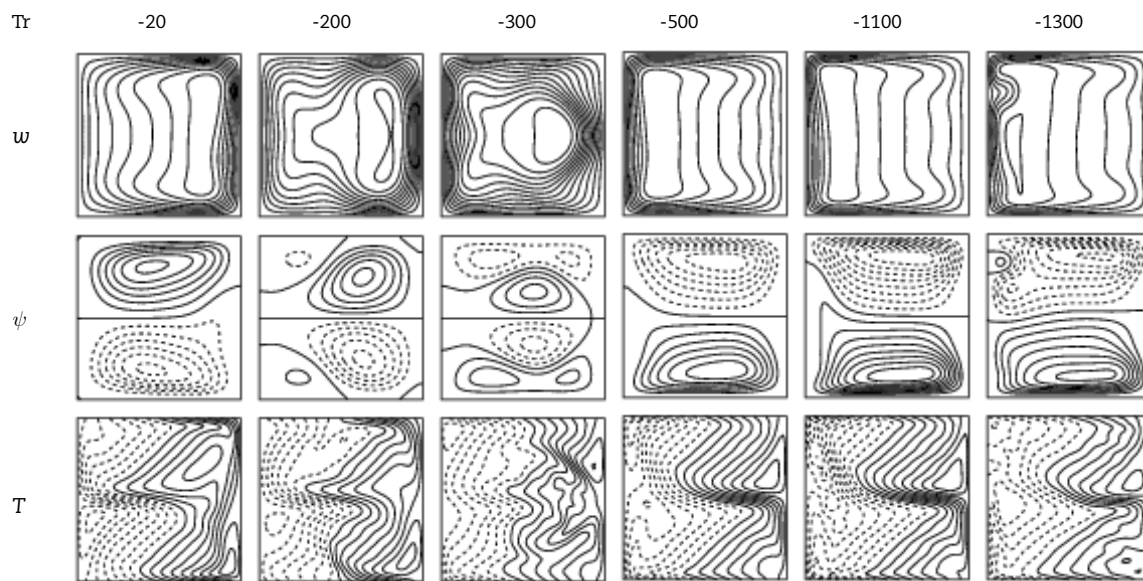
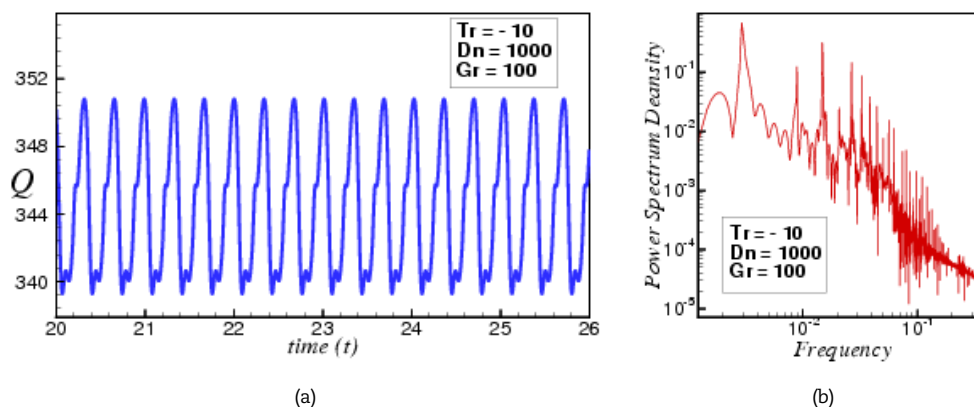
Time evolution calculation at $Tr = -10$ exposes the multi-periodic solution as shown in Fig. 4 (a) in *time vs. heat flux* plane. To understand more clearly about multi-periodic behavior, power spectrum density is further calculated as shown in Fig. 4 (b). It is noted that power spectrum density has enumerated in log scale. It is illustrated that the harmonics as well as its frequencies oscillated frequently. Two different velocity profiles such as axial (w) and secondary (ψ) flow and their isotherms (T) are shown in Fig. 5. Before interpreting the flow patterns, it is seen that two different types such as solid and dotted lines are found. The solid line is named as outward flow, constructed when it works at the anti-clockwise direction ($w, \psi, T \geq 0$). The dotted lines are addressed as the inward flow, operated when it works as clockwise direction ($w, \psi, T < 0$). However, the axial flow demonstrates that the flow velocity pushes to the inner wall of the duct. The secondary vortices explain that the vortices create at the outer wall of the duct. It is also observed from the secondary flow that the multi-periodic oscillation initiates consecutively after 30 seconds (See $t = 25.80$ to $t = 26.10$). It is moreover seen that there is an interaction between these flow velocities and the isotherms. If there is no high-velocity region in the axial flow, only two vortex asymmetric solutions are found in the secondary velocity. On the contrary, when the axial velocity consists of two high-velocity regions at the outer wall of the duct, at the same time, secondary velocity shows four vortex solutions. The newly (additional) two vortices are called Ekman vortex and the two vortices are named as Dean vortex. Moreover, when the velocity region at outer upper side is larger than the outer lower side, then the additional two vortices display that the lower vortex is smaller than the upper vortex. The isotherms narrate that the density of the streamlines is more at which the two high-velocity regions of axial flow and the four vortices of secondary flow are built up.

A significant change occurs if the Taylor number increases. Generally, chaotic oscillations come after periodic or multi-periodic oscillation as seen by many scholars' articles (Hasan et al. [16]). But the multi-periodic oscillation turns into steady-state in this instance. The steady state oscillation starts from $Tr = -182.50$ and continues to $Tr = -370.99$ which is also proved by linear stability analysis. Figure 6 (a) displays the unsteady behavior for $Tr = -190, -250$ & -370 respectively which is steady-state solution. Axial flow, secondary flow, and isotherms are shown in Fig. 6 (b). Two-, four-, six vortex solution is found for the respective Taylor numbers.



Table 2. Linear Stability of the negative solution for $\delta = 0.001$.

Tr	Q	σ_r	σ_i	Criteria
-10	450.71543312	1.394×10^1	2.61×10^1	Linearly Unstable
-182.49	416.62665602	1.109×10^1	0	Linearly Unstable
-182.50	412.35699527	-1.02×10^{-1}	0	Linearly Stable
-370.99	350.85006447	-1.1091	0	Linearly Stable
-371.00	350.67594665	4.2531	0	Linearly Unstable
-500	324.01841233	1.238×10^1	2.337×10^1	Linearly Unstable
-590.91	313.68463171	1.0345×10^1	0.0346	Linearly Unstable
-590.92	311.27454532	-0.020139	0	Linearly Stable
-912.12	287.22507638	-1.1091	0	Linearly Stable
-912.13	285.45369203	4.6798×10^1	-2.392×10^1	Linearly Unstable
-1000	282.17392705	7.625×10^1	-4.279×10^1	Linearly Unstable
-1500	262.02183223	1.136×10^2	6.568×10^1	Linearly Unstable

**Fig. 3.** Contours of axial velocity (topmost), stream function (central), isotherm (lowermost) for $Tr = -10, -250, -500, -1000, -1250, -1500$.**Fig. 4.** (a) Time dependent behavior in $t - Q$ plane, (b) Power spectrum density.

When Tr is crossed over 370.99, the steady-state solution converts into periodic oscillation as illustrated in Fig. 7 (a). The periodic oscillation is also well justified by the power spectrum density as shown in Fig. 7 (b). Two different types of flow velocity, axial and secondary flow, and isotherms are shown in Fig. 8. A dramatic change is observed in the flow velocities. From $Tr = -10$ to $Tr = -370.99$, the axial velocity pushes to the inner wall of the duct but from $Tr = -371$, the axial velocity pushes to the outer wall of the duct. Due to the change in the direction of axial velocity, the creation of the vortices changes, i.e., the vortices creates at the inner wall of the duct. Two-, three- and four-vortex solutions are found for the secondary flows.



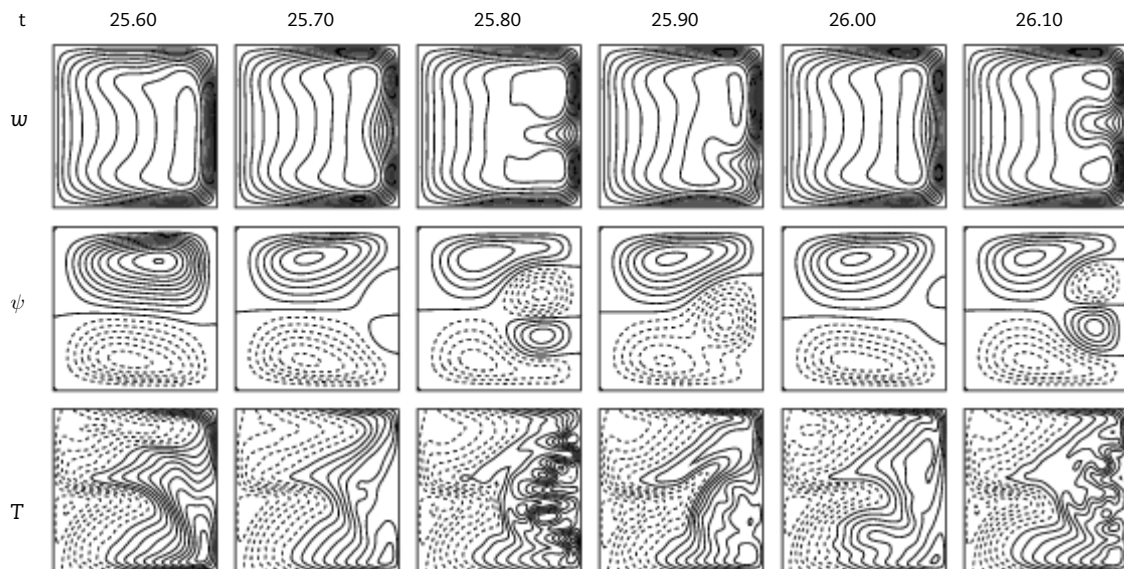
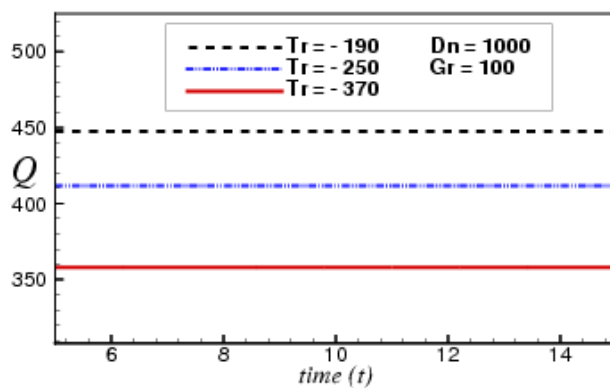
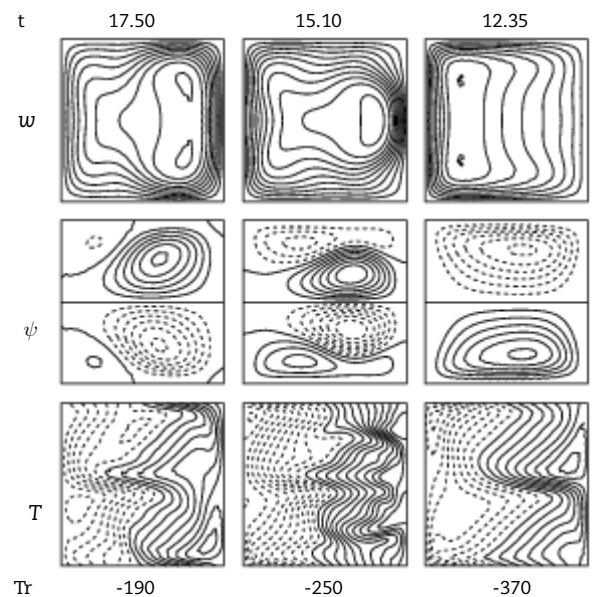


Fig. 5. Contours of axial velocity (topmost), stream function (middle), isotherm (lowermost) for $Tr=-10$.

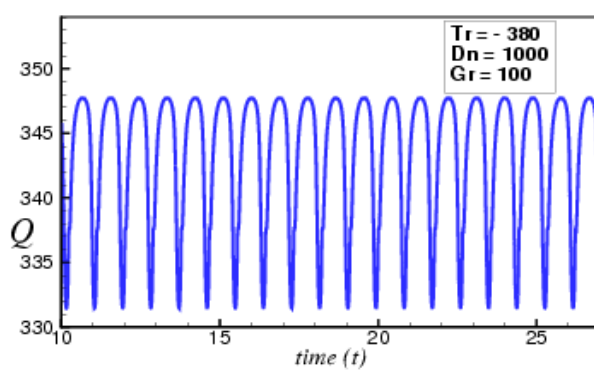


(a)

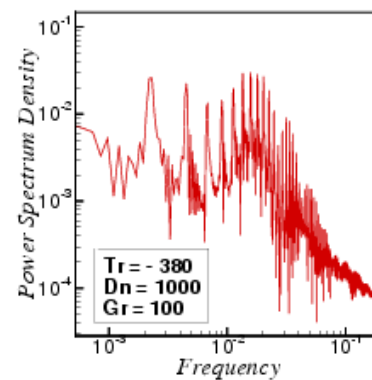


(b)

Fig. 6. (a) Time dependent behavior in $t - Q$ plane, (b) Contours of axial velocity (topmost), stream function (middle), isotherm (lowermost) for $Tr = -190, -250$ & -370 .



(a)



(b)

Fig. 7. (a) Time dependent behavior in $t - Q$ plane, (b) Power spectrum density.



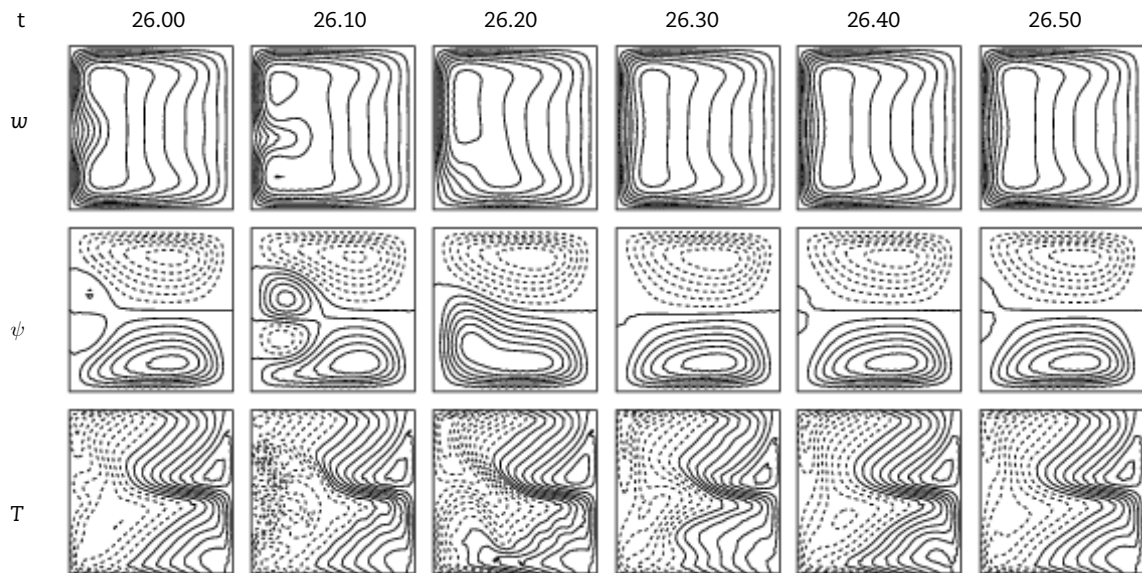


Fig. 8. Contours of axial velocity (topmost), stream function (middle), isotherm (lowermost) for $Tr=-380$.

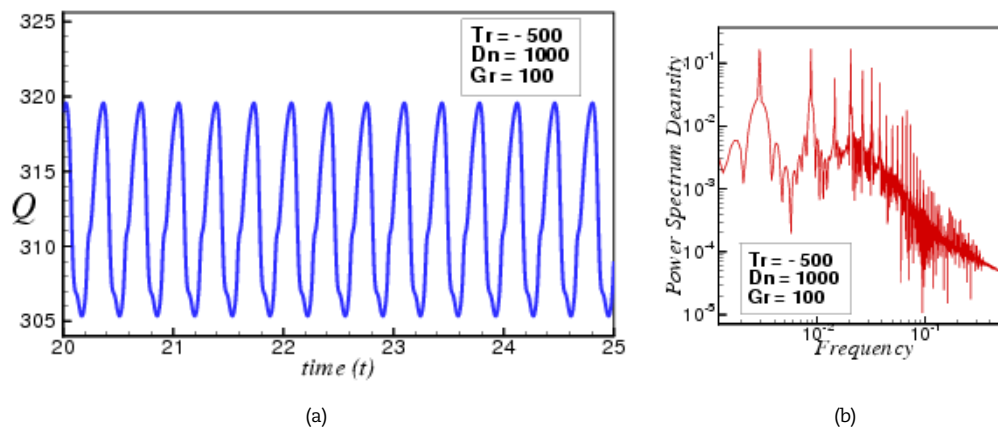


Fig. 9. (a) Time dependent behavior in $t - Q$ plane, (b) Power spectrum density.

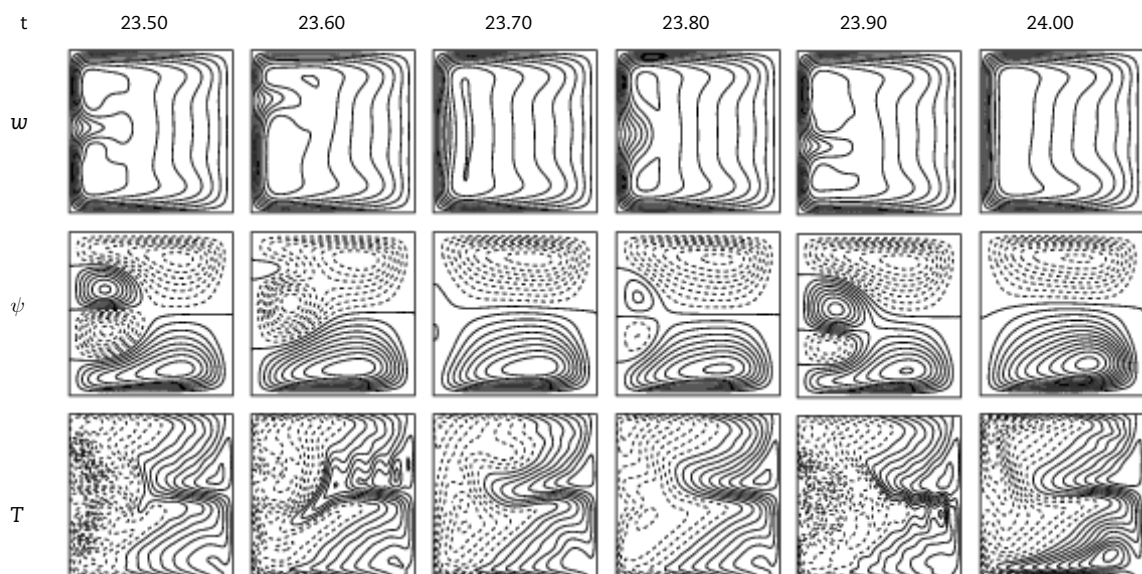


Fig. 10. Contours of axial velocity (topmost), stream function (middle), isotherm (lowermost) for $Tr=-500$.

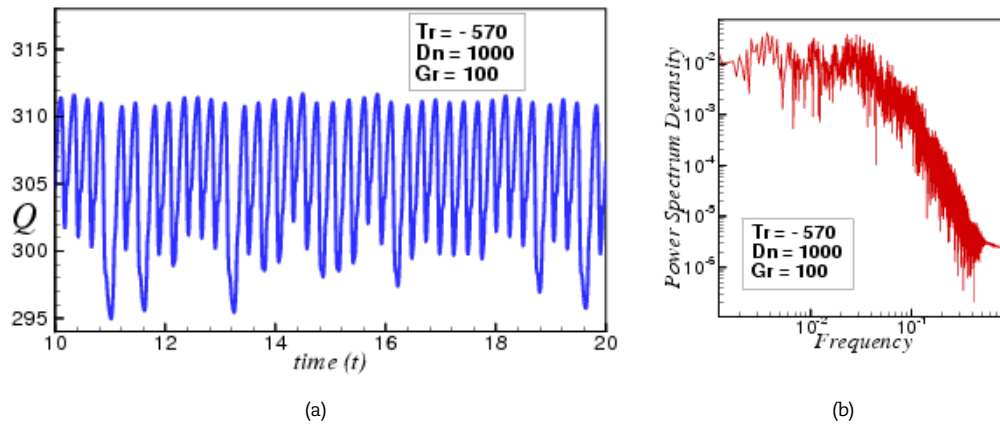


Fig. 11. (a) Time dependent behavior in $t - Q$ plane, (b) Power spectrum density.

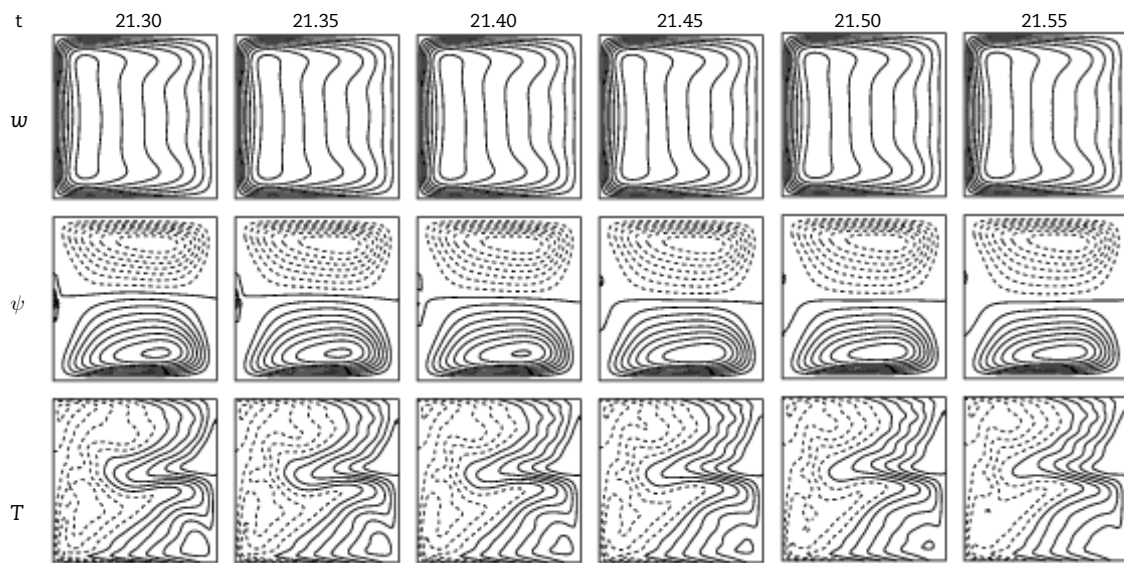


Fig. 12. Contours of axial velocity (topmost), stream function (middle), isotherm (lowermost) for $Tr=-570$.

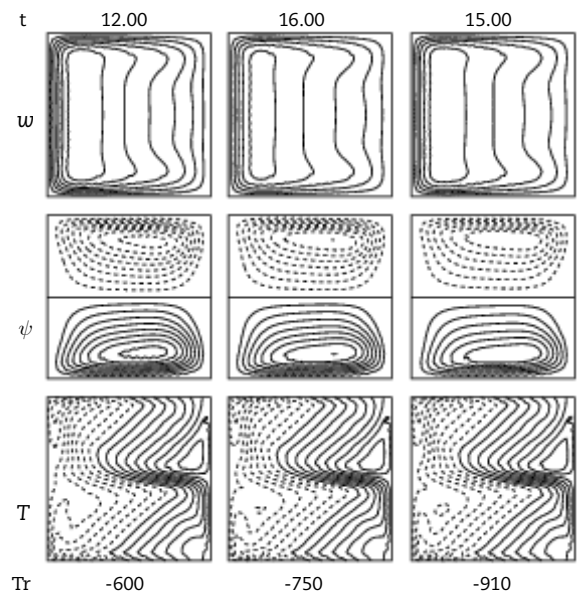
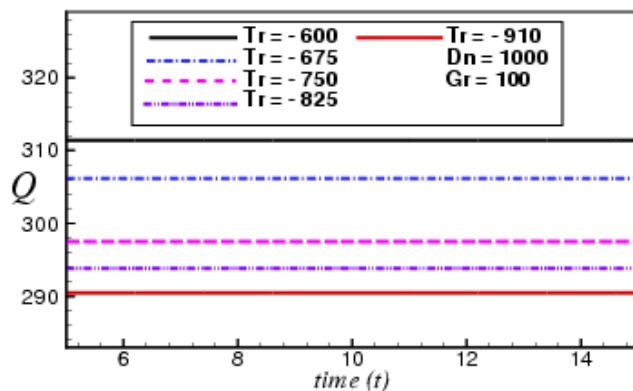


Fig. 13. (a) Time dependent behavior in $t - Q$ plane, (b) Contours of axial velocity (topmost), stream function (middle), isotherm (lowermost).



The vibration of the flow particle is increased if the Taylor number raises more. It is seen that at $Tr = -500$, the vibration is enhanced more than $Tr = -380$, and the vibrations as well as its frequencies is also analyzed by power spectrum density. Figures 9 (a) and 9 (b) show the time evolution calculation and the power spectrum density. Thus it is demonstrated from the figure that the multi-periodic solution has occurred at $Tr = -500$. Axial flow, secondary flow, and isotherms are shown in Fig. 10. Axial and secondary flows demonstrate that despite of the change of flow direction from $Tr = -380$, they behave in consisting of flow patterns are almost the same as in earlier ($-10 \leq Tr \leq -380$). More explicitly, at $t = 23.60$, it has seen that two high-velocity regions are created to the inner wall of the duct and the upper region is fewer than the lower region. For this reason, four vortex solution is found at the inner wall of the duct where among the two additional vortexes, the lower vortex is bigger than the upper vortex.

If the Taylor number has increased further, the flow oscillates irregularly, i.e, chaotic oscillation is occurred. At $Tr = -570$, chaotic oscillation is obtained as sketched in Fig. 11 (a). To ensure the chaotic oscillation, power spectrum density is also enumerated as shown in Fig. 11 (b). It has observed that because of the flow oscillation more in $t-Q$ plane, the harmonics have created irregular frequencies with a strong density. Axial flow, asymmetric two vortexes secondary flow, and isotherms are shown in Fig. 12.

Now, the transition of flow phenomena is calculated for further Taylor number in negative rotation and it is seen that from $Tr = -590.92$, the steady-state solution again starts and it is continued up to $Tr = -912.12$ which has also confirmed by the linear stability analysis. Figure 13 (a) explores the steady-state solutions for $Tr = -600, -675, -750, -825$ & -910 respectively. It is described from the figure that the magnitude of the heat flux is decreased for increasing the Taylor number. Axial flow, symmetric two vortexes secondary flow, and isotherms are shown in Figure 13 (b). It is observed that the flow velocity and the isotherms are the same whatever the Taylor number is.

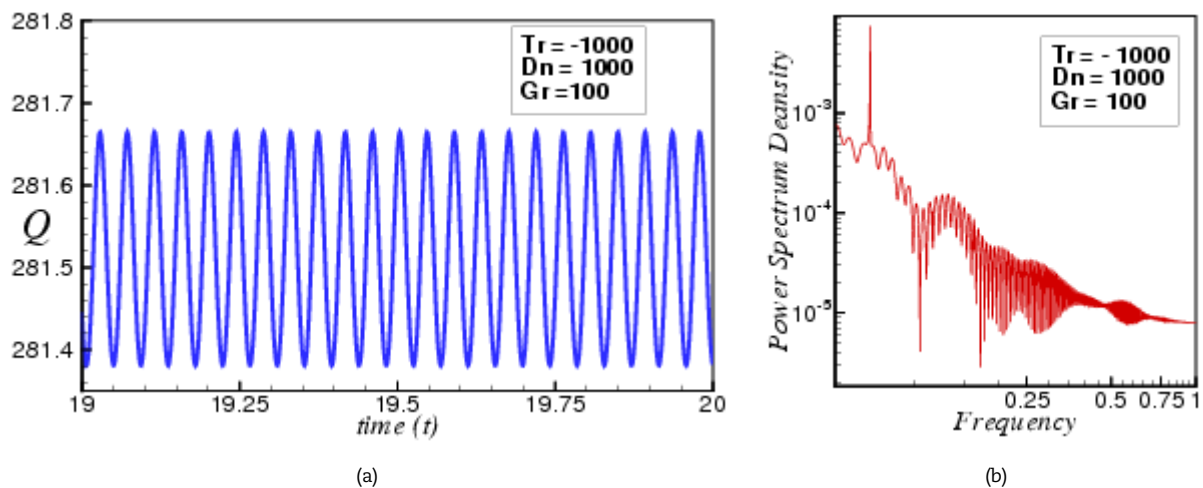


Fig. 14. (a) Time dependent behavior in $t-Q$ plane, (b) Power spectrum density.

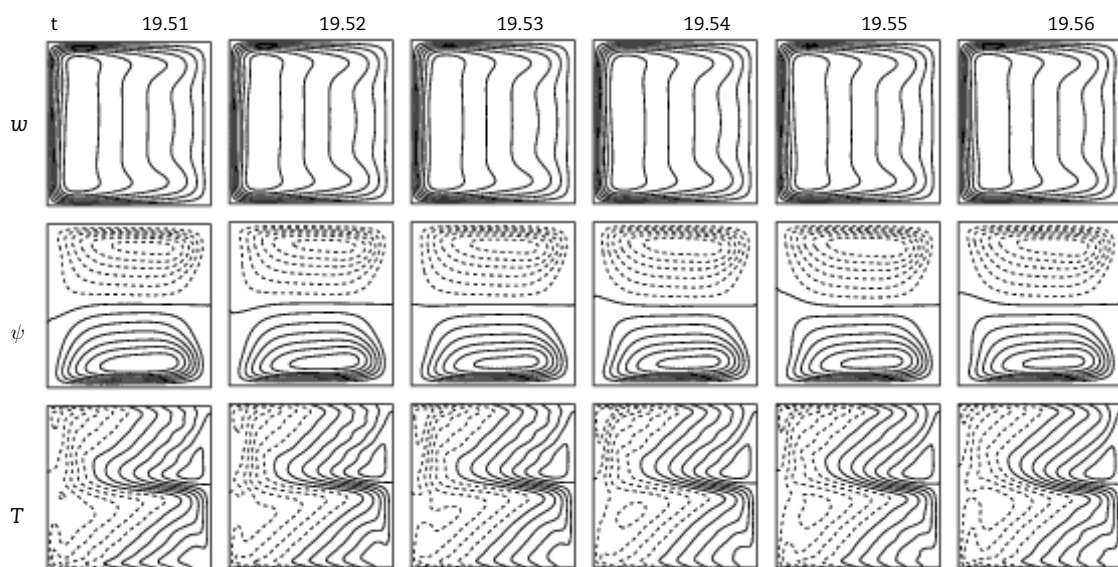


Fig. 15. Contours of axial velocity (topmost), stream function (middle), isotherm (lowermost) for $Tr=-1000$.



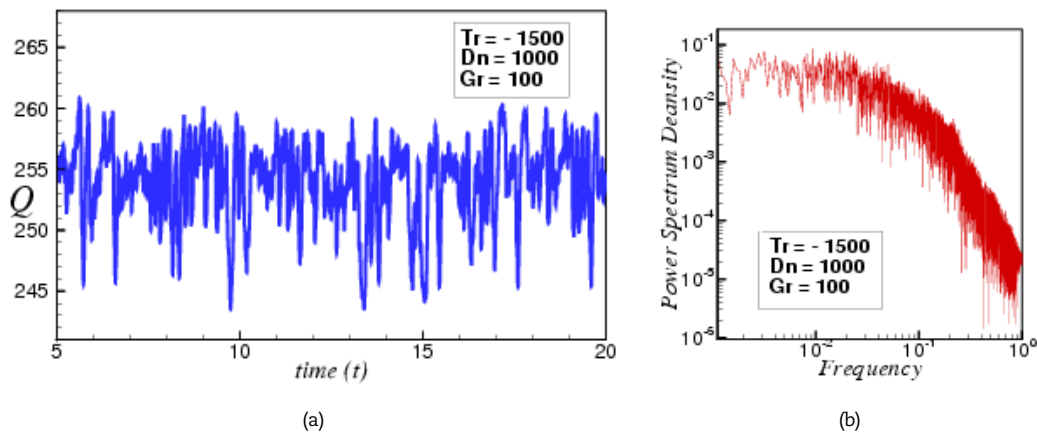


Fig. 16. (a) Time dependent behavior in $t-Q$ plane, (b) Power spectrum density.

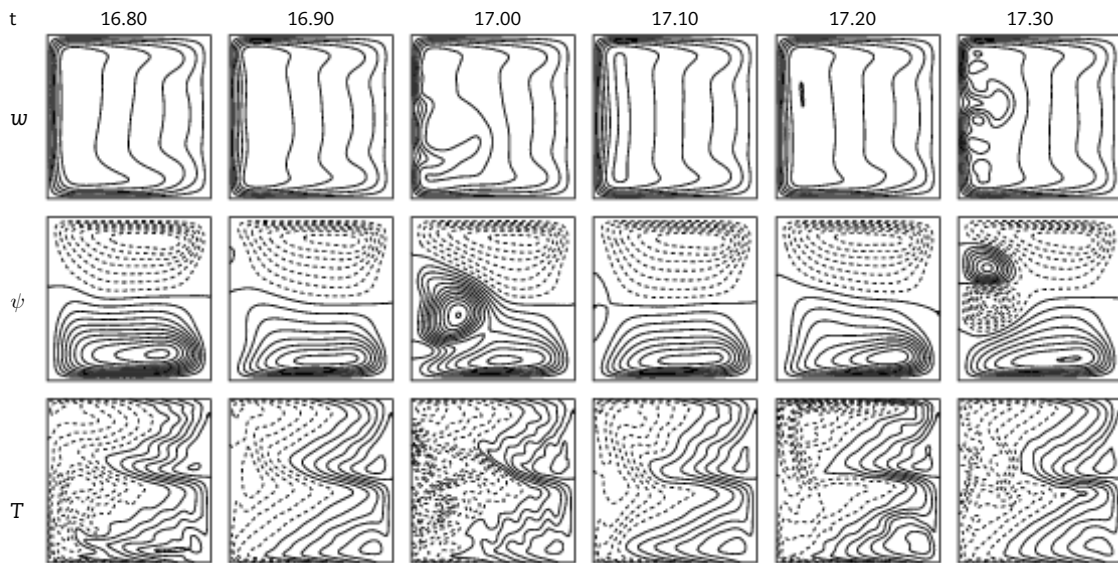


Fig. 17. Contours of axial velocity (topmost), stream function (middle), isotherm (lowermost) for $Tr = -1500$.

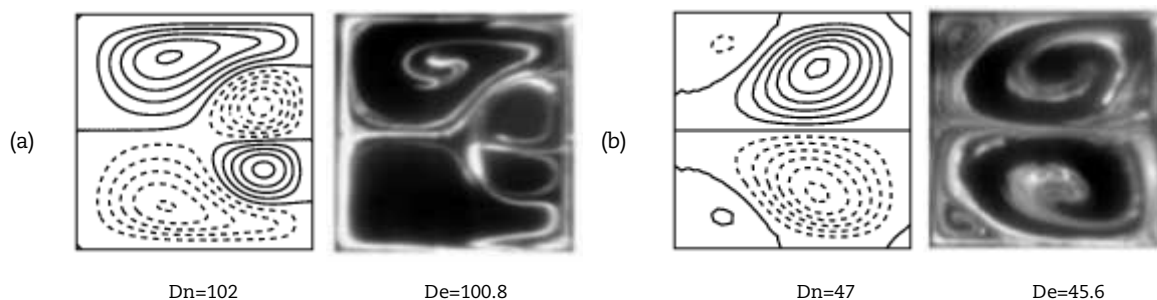


Fig. 18. Numerical vs. experimental results for rotating curved square duct flow at $Tr = -150$, (a) & (b) numerical result by the authors (left) and experimental result by Yamamoto et al. [31] (right).

The steady-state solution turns into a periodic solution from $Tr = -912.13$. Figures 14 (a) and 14 (b) represent the time-dependent solution and the power spectrum density for $Tr = -1000$ and it is certainly said that the unsteady solution shows periodic behavior. The oscillations and the frequencies illustrates that the oscillation and the frequency spectrum at $Tr = -1000$ are not stronger enough than $Tr = -380$. Because of the weaker oscillation, the axial flow, secondary flow, and isotherms are also influenced. The flow velocities and the isotherms are shown in Figure 15. It is seen that only two vortex asymmetric solutions are found for the Taylor number.

A dramatic phenomenon is found for raising Taylor number in the negative direction. As usual, multi-periodic oscillation starts after the periodic oscillation. But this is not happened between $-1000 \leq Tr \leq -1150$. The periodic oscillation directly converts into chaotic oscillation if the Taylor number is increased and this chaotic oscillation is continued up to $Tr = -1500$. Figures 16 (a) & 16 (b) depict the unsteady solution and the power spectrum for $Tr = -1500$. It is narrated that the oscillations are stronger more for growing up the Taylor number. The power spectrum density indicates that the line spectrum and its frequencies density has become enhanced more for increasing the Taylor number. Flow velocity such as axial flow and the secondary flow and isotherms are shown in Fig. 17. The axial flow demonstrates that the flow velocity creates strong velocity regions, as a consequence, two- up to four-vortex solutions have been found. The isotherms disclosed that the fluid has mixed and enhanced due to the rotation of the duct.



4.3 Numerical vs. experimental validation

To compare the numerical results with the experimental outcome express the accuracy of the computational work. Here, the numerical results presented in the present article have been also compared with the experimental data. Yamamoto et al. [31] was the only scholar who revealed the experimental outcomes only for the curved rotating duct of the square cross-section. In their investigation, they set up the mechanical instruments properly. In the water flow tank, they took dye which was mixed with alcohol so that the weight of water and dye were same. They injected the liquid with different pressure. A motor was included with the inner disk so that the duct was rotated in both positive and negative directions. After initiating the fluid flow through the curved duct, the motor was moved with angular velocity and then the flow phenomena captured with a camera. However, the experimental outcomes in Figure 18 found out by Yamamoto et al. [31] for negative rotation (fixed Taylor number, $Tr = -150$) with different pressure gradient. So, we have converted the value of the parameter same as their considering value. Then we have obtained some flow structures as seen in Figure 18. It is observed that the numerical results totally coincide with the experimental data.

5. Conclusion

A computational based investigation on curved rotating duct was presented in the ongoing exploration. At first, governing equations were presented, and then the numerical accuracy was checked. The numerical accuracy has ensured us that the collocation method was more reliable than the other methods. After that, linear stability of the curved square duct was searched for a comprehensive range of negative rotation, $-10 \leq Tr \leq -1500$; with curvature, $\delta = 0.001$ and Grashof number, $Gr = 100$. A connection between the linear stability and the unsteady solutions has also formed in this study. Moreover, the transition of the flow with respect to time for different Taylor numbers was performed. It was said that the unsteady flow undergoes through various flow transitions. The multi-periodic flows turned into chaotic via steady-state and periodic flows between $-10 \leq Tr \leq -570$. If the rotational parameter was risen up in negative direction further, it again converted into chaotic flow through the steady-state and periodic flow. Thus the scheme of the unsteady flows were written as, “multi-periodic \rightarrow steady-state \rightarrow periodic \rightarrow chaotic \rightarrow steady-state \rightarrow periodic \rightarrow chaotic.” For better confirmation of the vibrating flows in the unsteady solution, power spectrum density was disclosed. Two types of flow velocities, axial and secondary flow, and the temperature profiles were obtained for unsteady flows. It was described that for enhancing the temperature, the fluids have mixed. As a result, two vortex flows were grown up to six vortex flows. The secondary flows which were consisted of numerically were the same as the experimental result which has found by the other intellectual reviewer. This validation has ascertained us that the governing equation structure is completely correct.

Author Contributions

All authors planned the scheme, initiated the project, developed the mathematical modeling and examined the theory validation. The manuscript was written through the contribution of all authors. All authors discussed the results, reviewed and approved the final version of the manuscript.

Conflict of Interest

The authors declared no potential conflicts of interest with respect to the research, authorship and publication of this article.

Funding

The authors received no financial support for the research, authorship and publication of this article.

Nomenclature

D_n	Dean number	T	Temperature
Tr	Taylor number	u	Velocity components in the x-direction
Gr	Grashof number	v	Velocity components in the y-direction
h	Half height of the cross section	w	Velocity components in the z-direction
d	Half width of the cross section	x	Horizontal axis
L	Radius of the curvature	y	Vertical axis
Pr	Prandtl number	z	Axis in the direction of the main flow
t	Time	λ	Resistance coefficient

Greek Letters

δ	Curvature of the duct	ρ	Density
μ	Viscosity	κ	Thermal diffusivity
ν	Kinematic viscosity	ψ	Sectional stream function

References

- [1] Elsamni, O.A., Elsamni, A.A., El-Masry, O.A., Developing laminar flow in curved semi-circular ducts, *Alexandria Engineering Journal*, 58(1), 2019, 1-8. <https://doi.org/10.1016/j.aej.2018.03.013>
- [2] Du, W., Luo, L., Wang, S., Liu, J., Sundén, B., Heat transfer and flow structure in a rotating duct with detached pin fins, *Numerical Heat Transfer, Part A: Applications*, 75(4), 2019, 217–241. <https://doi.org/10.1080/10407782.2019.1580957>
- [3] Chandratilleke, T.T., Nadim, N., *Forced Convective Heat Transfer and Fluid Flow Characteristics in Curved Ducts*, An overview of heat transfer phenomena, Intech open sciences, 2012. <https://doi.org/10.5772/53064>
- [4] Mondal, R.N., Islam, M.S., Uddin, M.K., Hossain, M.A., Effects of Aspect Ratio on Unsteady Solutions through a Curved Duct Flow, *Applied Mathematics and Mechanics*, 34(9), 2013, 1-16. <https://doi.org/10.1007/s10483-013-1731-8>
- [5] Anand, R.B., Sandeep, R., Effect of Angle of Turn on Flow Characteristics of Y- Shaped Diffusing Duct Using CFD, *Frontiers in Automobile and mechanical Engineering, IEEE*, 2010. <https://doi.org/10.1109/FAME.2010.5714819>
- [6] Fiola, C., Agarwal, R.K., Simulation of Secondary and Separated Flow in Diffusing S Ducts, *Journal of Propulsion and Power*, 31(1), 2015, 180-191.




<https://doi.org/10.2514/1.B35275>


- [7] Rumsey, C.L., Gatski, T.B., Morrison, J.H., Turbulence Model Predictions of Strongly Curved Flow in a U-Duct, *AIAA Journal*, 38(8), 2000, 1394-1402. <https://doi.org/10.2514/2.1115>
- [8] Chamkha, A., Ismael, M., Kasaeipoor, A., Armaghani, T., Entropy Generation and Natural Convection of CuO-Water Nanofluid in C-Shaped Cavity under Magnetic Field, *Entropy*, 18(2), 2016, 1-18. <https://doi.org/10.3390/e18020050>
- [9] Nowruzi, H., Ghassemi, H., Nourazar, S.S., Study of the effects of aspect ratio on hydrodynamic stability in curved rectangular ducts using energy gradient method, *Engineering Science and Technology, an International Journal*, 23(2), 2019, 334-344. <https://doi.org/10.1016/j.jestch.2019.05.004>
- [10] Watanabe, T., Yanase, S., Bifurcation Study of Three-Dimensional Solutions of the Curved Square-Duct Flow, *Journal of the Physical Society of Japan*, 82(074402), 2013, 1-9. <https://doi.org/10.7566/JPSJ.82.074402>
- [11] Mondal, R.N., Kaga, Y., Hyakutake, T., Yanase, S., Bifurcation Diagram for Two-dimensional Steady Flow and Unsteady Solutions in a Curved Square Duct, *Fluid Dynamics Research*, 39, 2007, 413-446. <https://doi.org/10.1016/j.fluiddyn.2006.10.001>
- [12] Nazeer, G., Shams-ul-Islam, Shigri, S.H., Saeed, S., Numerical investigation of different flow regimes for multiple staggered rows, *AIP Advances*, 9(035247), 2019. <https://doi.org/10.1063/1.5091668>
- [13] Krishna, C.V., Gundiah, N., Arakeri, J.H., Separation and secondary structures due to unsteady flow in a curved pipe, *Journal of Fluid Mechanics*, 815, 2017, 25-59. <https://doi.org/10.1017/jfm.2017.7>
- [14] Islam, M.Z., Mondal, R.N., Rashidi, M.M., Dean-Taylor Flow with Convective Heat Transfer through a Coiled Duct, *Computers & Fluids*, 149, 2017, 41-55. <https://doi.org/10.1016/j.compfluid.2017.03.001>
- [15] Sultana, M.N., Hasan, M.S., Mondal, R.N., A numerical study of unsteady heat and fluid flow through a rotating curved channel with variable curvature, *AIP Conference Proceedings*, 2121 (030009), 2019. <https://doi.org/10.1063/1.5115854>
- [16] Hasan, M.S., Islam, M.M., Ray, S.C., Mondal, R.N., Bifurcation structure and unsteady solutions through a curved square duct with bottom wall heating and cooling from the ceiling, *AIP Conference Proceedings*, 2121 (050003), 2019. <https://doi.org/10.1063/1.5115890>
- [17] Wang, L., Pang, O., Cheng, L., Bifurcation and stability of forced convection in tightly coiled ducts: stability, *Chaos, Solitons and Fractals*, 27, 2006, 991-1005. <https://doi.org/10.1016/j.chaos.2005.04.066>
- [18] Chamkha, A.J., Al-Mudhaf, A., Unsteady heat and mass transfer from a rotating vertical cone with a magnetic field and heat generation or absorption effects, *International Journal of Thermal Sciences*, 44, 2005, 267-276. <https://doi.org/10.1016/j.ijthermalsci.2004.06.005>
- [19] Yanase, S., Mondal, R.N., Kaga, Y., Numerical study of non-isothermal flow with convective heat transfer in a curved rectangular duct, *International Journal of Thermal Science*, 44, 2005, 1047-60. <https://doi.org/10.1016/j.ijthermalsci.2005.03.013>
- [20] Islam, M.N., Ray, S.C., Hasan, M.S., Mondal, R.N., Pressure-driven flow instability with convective heat transfer through a rotating curved rectangular duct with differentially heated top and bottom walls, *AIP Conference Proceedings*, 2121 (030011), 2019. <https://doi.org/10.1063/1.5115856>
- [21] Ray, S.C., Hasan, M.S., Mondal, R.N., On the Onset of Hydrodynamic Instability with Convective Heat Transfer Through a Rotating Curved Rectangular Duct, *Mathematical Modelling of Engineering Problems*, 7(1), 2020, 31-44. <https://doi.org/10.18280/mmep.070105>
- [22] Dean, W.R., Note on the motion of fluid in a curved pipe, *Philos Mag*, 4, 1927, 208-23. <https://doi.org/10.1080/14786440708564324>
- [23] Harding, B., Stokes, Y.M., Bertozzi, A.L., Effect of inertial lift on a spherical particle suspended in flow through a curved duct, *Journal of Fluid Mechanics*, 25, 2019, 1-43. <https://doi.org/10.1017/jfm.2019.323>
- [24] Nowruzi, H., Ghassemi, H., Nourazar, S.S., Hydrodynamic stability study in a curved square duct by using the energy gradient method, *Journal of the Brazilian Society of Mechanical Sciences and Engineering*, 41, 2019, 1-20. <https://doi.org/10.1007/s40430-019-1790-z>
- [25] Kabanemi, K.K., Marcotte, J.P., Numerical Simulation of Suction Blow Molding Process for Producing Curved Ducts, *Polymer engineering and science*, Wiley online library, 59(2), 2020, 1-17. <https://doi.org/10.1002/pen.24939>
- [26] Parvin, S., Nasrin, R., Alim, M.A., Hossain, N.F., Chamkha, A.J., Thermal conductivity variation on natural convection flow of water-alumina nanofluid in an annulus, *International Journal of Heat and Mass Transfer*, 55(19-20), 2012, 5268-5274. <https://doi.org/10.1016/j.ijheatmasstransfer.2012.05.035>
- [27] Mondal, R.N., Watanabe, T., Hossain, M.A., Yanase, S., Vortex-Structure and Unsteady Solutions with Convective Heat Transfer Through a Curved Duct, *Journal of Thermophysics and Heat Transfer*, 31(1), 2017, 243-254. <https://doi.org/10.2514/1.T4913>
- [28] Dolon, S.N., Hasan, M.S., Ray, S.C., Mondal, R.N., Vortex-structure of secondary flows with effects of strong curvature on unsteady solutions through a curved rectangular duct of large aspect ratio, *AIP Conference Proceedings*, 2121(050004), 2019. <https://doi.org/10.1063/1.5115891>
- [29] Arifuzzaman, M., Islam, M.M., Paul, S.K., Mondal, R.N. Pressure-driven Flow Instability with Convective Heat Transfer through a Rotating Curved Square Duct with Strong Curvature, *Current Journal of Applied Science and Technology*, 23(2), 2017, 1-18. <https://doi.org/10.9734/CJAST/2017/31612>
- [30] Yanase, S., Watanabe, T., Hyakutake, T., Traveling-wave solutions of the flow in a curved-square duct, *Physics of Fluids*, 20, 2008, 124101. <https://doi.org/10.1063/1.3029703>
- [31] Yamamoto, K., Wu, X., Nozaki K., Hayamizu, Y., Visualization of Taylor-Dean flow in a curved duct of square cross-section, *Fluid Dynamics Research*, 38, 2006, 1-18. <https://doi.org/10.1016/j.fluiddyn.2005.09.002>
- [32] Nivedita, N., Ligrani, P., Papautsky, I., Dean Flow Dynamics in Low-Aspect Ratio Spiral Microchannels, *Scientific Reports*, 7, 2017, 44072. <https://doi.org/10.1038/srep44072>
- [33] Mondal, R.N., Kaga, Y., Hyakutake, T., Yanase, S., Effects of curvature and convective heat transfer in curved square duct flows, *Trans. ASME, Journal of Fluids Engineering*, 128 (9), 2006, 1013-1022. <https://doi.org/10.1115/1.2236131>
- [34] Hasan, M.S., Mondal, R.N., Kouchi, T., Yanase, S. Hydrodynamic instability with convective heat transfer through a curved channel with strong rotational speed, *AIP Conference Proceedings*, 2121 (030006), 2019. <https://doi.org/10.1063/1.5115851>
- [35] Umavathi, J.C., Chamkha, A.J., Mateen, A., Al-Mudhaf, A., Unsteady two-fluid flow and heat transfer in a horizontal channel, *Heat Mass Transfer*, 42, 2005, 81-90. <https://doi.org/10.1007/s00231-004-0565-x>
- [36] Chandratilleke, T.T., Nadim, N., Narayanaswamy, R., Vortex structure-based analysis of laminar flow behaviour and thermal characteristics in curved ducts, *International Journal of Thermal Sciences*, 59, 2012, 75-86. <https://doi.org/10.1016/j.ijthermalsci.2012.04.014>
- [37] Hasan, M.S., Mondal, R.N., Lorenzini, G., Numerical Prediction of Non-isothermal Flow with Convective Heat Transfer Through a Rotating Curved Square Channel with Bottom Wall Heating and Cooling from the Ceiling, *International Journal of Heat and Technology*, 37 (3), 2019, 710-726. <https://doi.org/10.18280/ijht.370307>
- [38] Hasan, M.S., Mondal, R.N., Lorenzini, G., Centrifugal Instability with Convective Heat Transfer Through a Tightly Coiled Square Duct, *Mathematical Modelling of Engineering Problems*, 6 (3), 2019, 397-408. <https://doi.org/10.18280/mmep.060311>

ORCID iD

Mohammad Sanjeed Hasan  <https://orcid.org/0000-0003-2960-5524>

Shamsun Naher Dolon  <https://orcid.org/0000-0003-0497-1915>

Rabindra Nath Mondal  <https://orcid.org/0000-0001-6596-575X>

Giulio Lorenzini  <https://orcid.org/0000-0002-5676-8575>



© 2021 Shahid Chamran University of Ahvaz, Ahvaz, Iran. This article is an open access article distributed under the terms and conditions of the Creative Commons Attribution-NonCommercial 4.0 International (CC BY-NC 4.0 license) (<http://creativecommons.org/licenses/by-nc/4.0/>).

How to cite this article: Hasan M.S., Dolon S.N., Chakraborty H.S., Mondal R.N., Lorenzini G. Numerical Investigation on Flow Transition through a Curved Square Duct with Negative Rotation, *J. Appl. Comput. Mech.*, 7(3), 2021, 1435-1447. <https://doi.org/10.22055/JACM.2020.33606.2253>

